Aerosol and Air Quality Research, 19: 2827–2843, 2019

ISSN: 1680-8584 print / 2071-1409 online
doi: 10.4209/aaqr.2019.04.0187

Source Identification of Episodic Rain Pollutants by a New Approach: Combining Satellite Observations and Backward Air Mass Trajectories

Ismail Anil, Omar Alagha*, Nawaf I. Blaisi, Iehab Abdelilah Mohamed, Mohammad Hisham Barghouthi, Mohammad Saood Manzar

Department of Environmental Engineering, College of Engineering, Imam Abdulrahman Bin Faisal University, Dammam, Saudi Arabia

ABSTRACT

In this study, various source apportionment methods, viz., enrichment factor, relative source contribution, and factor analysis in addition to cluster analysis coupled with satellite observations, were used to investigate the origin of rainwater pollutants in an arid urban area of Saudi Arabia. The rainwater samples were collected by an automatic wet-only sequential rain sampler and analyzed for their pH, electrical conductivity (EC), and major ions (Cl^-, NO_3^-, SO_4^{2-}, HCO_3^-, Na^+, K^+, NH_4^+, Ca^{2+}, and Mg^{2+}). The results revealed that the chemical composition was dominated by Ca^{2+}, SO_4^{2-}, Cl^-, HCO_3^-, and Na^+, which represented 80% of the total ionic equivalent concentration. Ca^{2+}, the most abundant ion, exhibited a mean concentration of 480 μeq L^{-1} and accounted for 30% of the total ionic equivalent concentration. The study area received a total ionic wet deposition flux (F_{WD}) of 4.07 tons km^{-2} y^{-1}, and SO_4^{2-} and NO_3^- contributed 76% and 24%, respectively, of the rainwater acidity. Ca^{2+} was responsible for 80% of the rainwater's neutralization. The source apportionment indicated that intense local human activity and medium- to long-range transport from Kuwait, Iraq, Qatar, Riyadh, and the Western Province produced the majority of the anthropogenic components (SO_4^{2-}, NO_3^-, and NH_4^+), which represented 47% of the total ionic F_{WD}. However, moderate to high particulate matter loads over the southern part of Saudi Arabia and long-range transport from Iraq and Kuwait contributed the crustal components (Ca^{2+}, HCO_3^-, K^+, and Mg^{2+}), which accounted for 36% of the total ionic F_{WD}, whereas the Arabian Gulf was the primary source of the marine components (Na^+ and Cl^-). We found combining satellite observations and cluster analysis of backward air mass trajectories to be an effective new approach for assessing the source-receptor relationships for atmospheric air pollutants.

Keywords: Source apportionment; Backward trajectory; Cluster analysis; Satellite observation; Rainwater chemical composition; Wet deposition flux.

INTRODUCTION

The rapid development in urban areas could lead to serious air pollution concerns that affect millions of people around the world. Huge amounts of anthropogenic pollutants enter the atmosphere every instant via fossil fuel burning or from major power generation activities and industrial processes, which further lead to the development of unwanted gaseous pollutants such as oxides of sulfur and nitrogen in the atmosphere (Li *et al.*, 2016; Wu *et al.*, 2018). Thereafter, these gases are converted to strong acids, namely sulfuric and nitric acid, by gas-to-particle conversion, and they ultimately contribute to the formation of acid rain (Al-Momani *et al.*, 2000; Başak and Alagha, 2004; Gaga and Ari, 2011; Burns *et al.*, 2016).

Air pollutants are removed from the atmosphere by wet deposition and dry deposition processes (Likens, 1987; Budhavant *et al.*, 2009; Tsai *et al.*, 2014). Wet deposition is the main route and a powerful mechanism for the scavenging of the two phases, namely the gaseous and the particulate phase (Facchini Cerqueira *et al.*, 2014). The deposition could be very acidic which may harm habitats and ecology systems by soil acidification and excess level of nitrogen leading to eutrophication (Driscoll, 2001; Bouwman *et al.*, 2002; EMEP, 2013).

The rainwater chemical composition can reveal significant information on the degree of pollution and could help to assess the atmospheric deposition and transport of acidifying, neutralizing, and eutrophying species, heavy metals, and aerosols (Alagha and Tuncel, 2003; Tiwari *et al.*, 2016; Anil *et al.*, 2017). Furthermore, statistical evaluation of rainwater chemical composition data can provide insights into the necessary control and management practices to reduce and mitigate air pollution (Alagha and Tuncel, 2003; Başak and

* Corresponding author.
Tel.: +966133331682, Fax: +966133330240
E-mail address: oaga@iau.edu.sa

Alagha, 2004; Akkoyunlu *et al.*, 2011). The study of rainwater chemical composition has been proven to be a powerful and reliable methodology to assess atmospheric pollution and its environmental impacts (Alagha and Tuncel, 2003; Al-Khashman, 2009; Akkoyunlu *et al.*, 2011; Romero Orué *et al.*, 2019; Vlastos *et al.*, 2019).

Rain scarcity is a challenge to agricultural activities in the arid and semiarid regions (Whelpdale *et al.*, 1997; DeNicola *et al.*, 2015). Saudi Arabia is recognized by its arid and harsh weather with very scarce rainfall throughout the year (Al-Refeai and Al-Ghamdy, 1994; Mashat and Abdel Basset, 2011). There are very few studies in arid regions such as Saudi Arabia regarding rainwater chemistry and its association with the environment or atmosphere (Ahmed *et al.*, 1990; Schemenauer and Cereceda, 1992; Alabdula'aly and Khan, 2000; Wedyan, 2013; Michelsen *et al.*, 2015). Previous research points that the nature of the water collected from rain or wet deposition was mostly alkaline and partially acidic. Some of the studies in western regions of Saudi Arabia pinpointed the presence of terrestrial fungi in most of the rain samples (Nasser, 2005). In addition to these, other researchers investigated the occurrence and sources of polycyclic aromatic hydrocarbons in rainwater (Al-Daghri *et al.*, 2013; Al-Saleh *et al.*, 2013; Al-Daghri *et al.*, 2014).

Air mass back trajectories could provide insights into the source regions contributing to concentrations of monitored air pollutants at a receptor site if the emission inventories of the potential source regions are well known (Kant *et al.*, 2019). In practical application, presence or access to those kinds of datasets may not be straightforward. In that case, an alternative approach combining satellite observations and backward air mass trajectories could procure a better understanding of the source-receptor relationship for atmospheric air pollutants. Notaro *et al.* (2013) investigated the trajectory analysis of Saudi Arabian dust storms by utilizing weather observations and remotely sensed aerosol optical depth (AOD). The current study deals with remotely sensed air pollutants data such as AOD, NO_2, SO_2, and sea salt. The new addition in the current study is that it used the real-time measurements of pollutants from collected rainwater along with remotely sensed satellite data. The main objective of this study is to identify the sources affecting the elevated rainwater pollutants using statistical models including enrichment factor, relative source contribution, factor analysis, and cluster analysis. The approach of combining satellite observations and cluster analysis of backward air mass trajectories of rainy days was used as a tool in investigating the source-receptor relationship for rainwater pollutants.

MATERIALS AND METHODS

Study Area and Sampling Methodology

The study area Dammam is the largest city in the Eastern Province Region of Saudi Arabia with an area of 800 km^2 and a population of about 1.3 million inhabitants. It is also considered as the major center for oil, commerce, and the petrochemical industry. The urbanized part of the Dammam metropolitan area is approximately 912 km^2 and the land use is distributed as follows: 36% residential and commercial, 32% zoning area, 19% industrial, and 13% seaports and airports. The study area receives 7–10 severe dust storms per year. During these episodic events, atmosphere of the study area is highly enriched with mineral particles when strong winds lift these particles from the regional soil which is reported to be composed of alluvium of gravel, sand, silt, clay deposits, and limestone subsoil (Alsaaran, 2008; El-Mubarak *et al.*, 2014). The temperature is rarely below 7°C or above 46°C and usually ranges between 11°C and 44°C with an annual average of 28°C. The rainy season is typically between mid-October and mid-May with an average annual precipitation total of 100 ± 8 mm (Mashat and Abdel Basset, 2011). Accordingly, the precipitation regime of the region is categorized as "arid". Wind systems from northern directions dominate over the area with an average ground-level wind speed of 4.2 m s^{-1}.

The rain sampling was conducted at the air quality monitoring station located in the main campus of Imam Abdulrahman Bin Faisal University (26.390°N, 50.182°E). The station is 6.7 m above the sea level and 2 km away from the coastline. The location of the air quality monitoring station and the land use map of the study area are shown in Fig. 1. An Eigenbrodt® automatic wet-only sequential rain sampler was used. The total height and collection surface area of the sampler are 1.6 m and 500 cm^2, respectively. The sampler had been operated continuously during the rainy season between October 2015 and May 2016. The start time of the sampling was set to 09:00 a.m. as it is recommended (GAW, 2004). A total number of 21 rainwater samples were collected between November 11th and April 17th with a total precipitation depth of 74.4 mm.

Chemical Analysis

The pH and electrical conductivity (EC) measurements of the samples were performed immediately after the sample collection by using Consort™ C3010 Benchtop Multiparameter Analyzer. Following this, each sample was filtered through a 0.45-µm cellulose acetate membrane filter using a Nalgene® filtration system. The filtrate part (soluble fraction) of the sample was transferred into a Nalgene® bottle, sealed tightly, and stored in a refrigerator at 4°C prior to the time of analysis. Major anions (Cl^-, NO_3^-, and SO_4^{2-}) and cations (Na^+, K^+, NH_4^+, Ca^{2+}, and Mg^{2+}) were quantified within a week after sample collection by using a high-performance liquid chromatograph (Prominence; Shimadzu). Bicarbonate ion (HCO_3^-) in rainwater samples were determined using Standard Methods: 2320 B. Titration Method.

Quality Assurance Measures

The field and laboratory blanks were prepared to correct the possible contaminations of the samples during the sampling, handling, preparation, storage, and measurement steps. Field blanks were collected bimonthly by routine washing of the rainwater collection bucket with 100-mL ultrapure water. Laboratory blanks were prepared and carried through the same procedure as the samples along with each filtration set. The blanks were treated as a real sample and included in all analyses. The ultrapure water with a resistivity of 18.2 MΩcm used in rinsing, blank

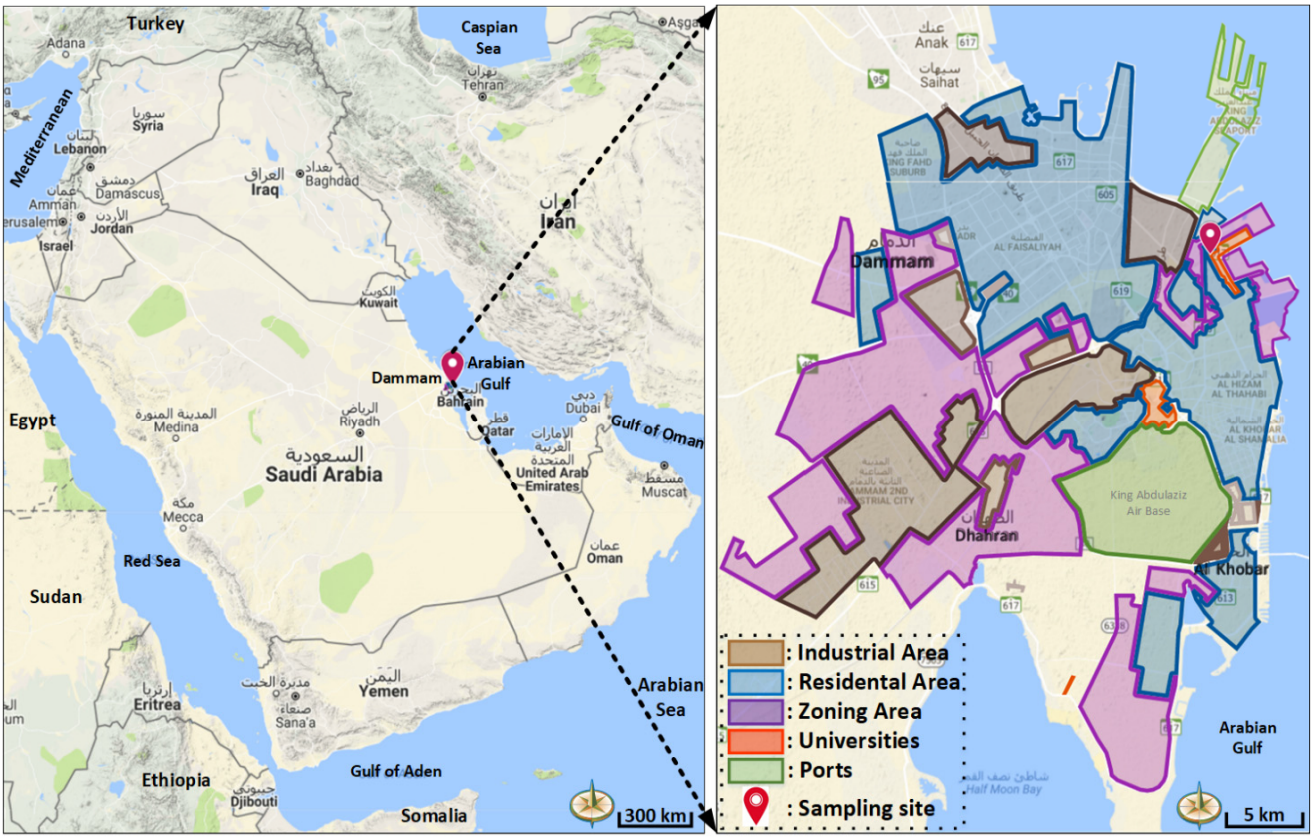

Fig. 1. Location of the sampling site and the land use map of the study area.

preparation, dilution, and calibration steps was produced by an ELGA® water purification system.

The detection limit (DL) of each analyte measured in rainwater samples was calculated to be mean of the blank values plus three times the standard deviation of the blank values (de Moraes Dias, *et al.*, 2012). The analytical protocols were verified before measurements of the samples by analyzing Standard Reference Materials (SRMs; simulated rainwater SR-1 and SR-2; High-Purity Standards®). The precision of each method was determined by calculating the relative standard deviation (RSD; %) of 10 replicate measurements of the standards and samples. The possible contaminations of the samples were checked by blank to sample ratios. The calibration range, linearity (the coefficient of determination (R^2) of the calibration), DL, precision (%), and sample to blank ratio (S/B) of each analyte are indicated in Table 1.

The calculated linearities ranging from 0.9989 to 0.9998 were found to be acceptable. The analyte concentration per sample was substantially higher than its DL. The precision results varying between 1.23% and 9.29% were satisfactory. S/B ratios were above 3, suggesting that the contaminations of the samples were negligible.

The equivalent ratio of the total anions to total cations ($\sum_{anions}/\sum_{cations}$) has been used as an indication of the analytical data quality and completeness of measured parameters (Al-Momani *et al.*, 1995a, b). If this ratio is within the interval of 1 ± 0.25, data are commonly assumed acceptable (Keene *et al.*, 1986). The mean $\sum_{anions}/\sum_{cations}$ ratio for the collected samples is 0.94 ± 0.34, suggesting that most of the important ions were included in measurements.

Data Analysis

Volume weighted mean (VWM) values are commonly used to avoid such variability in measured parameters due to precipitation amount. Wet deposition flux (F_{WD}) could be defined as the deposited amount of atmospheric chemicals onto unit area of Earth's surface via hydrometeorological processes. The VWM concentration and F_{WD} of pollutants in rainwater were calculated by using Eqs. (1) and (2), respectively (Alagha and Tuncel, 2003):

$$C_{VWM} = \sum_{i=1}^{n}[X_i]P_i \Big/ \sum_{i=1}^{n} P_i \quad (1)$$

where C_{VWM} is the VWM concentration, $[X_i]$ is the concentration of an ion in the i^{th} rainwater sample, P_i is the rainfall depth (mm) during the i^{th} rain event, and:

$$F_{WD} = [X_i]\, P_i / A \quad (2)$$

where F_{WD} was calculated as mg m^{-2} or kg km^{-2} and A is the collection surface area of the sampler.

Marine and crustal enrichment factors are commonly practiced in identifying marine and crustal sources of the ions in rainwater, respectively. Marine enrichment factor (EF_m) is calculated using Na^+ as a reference for marine source (Eq. (3)) (Kulshrestha *et al.*, 1996), while crustal enrichment

Table 1. Quality control performances of measured ions.

Ion	Calibration range[a]	Linearity (R^2)	DL[a]	Precision (%)	S/B
Na^+	0–25	0.9991	0.020	4.14	126
K^+	0–2.5	0.9989	0.050	4.92	7.88
Ca^{2+}	0–50	0.9997	0.150	5.10	109
Mg^{2+}	0–2.5	0.9993	0.050	5.44	5.79
NH_4^+	0–5.0	0.9991	0.150	2.55	20.3
HCO_3^-	0–50	0.9990	0.130	3.25	35.2
Cl^-	0–25	0.9998	0.200	4.29	34.4
NO_3^-	0–25	0.9998	0.180	3.06	49.1
SO_4^{2-}	0–50	0.9991	0.340	5.08	64.2

[a] Calibration range and DL are in mg L^{-1}.

factor (EF_c) is determined using Ca^{2+} as a reference for crustal source (Eq. (4)) (Al-Momani *et al.*, 1997):

$$EF_m = [X/Na^+]_{rain}/[X/Na^+]_{sea} \quad (3)$$

$$EF_c = [X/Ca^{2+}]_{rain}/[X/Ca^{2+}]_{crust} \quad (4)$$

where $[X/Na^+]_{rain}$ and $[X/Na^+]_{sea}$ are the ratios of concentration of an ion (X) to Na^+ concentration in rainwater sample and seawater, respectively, and $[X/Ca^{2+}]_{rain}$ and $[X/Ca^{2+}]_{crust}$ are the ratios of concentration of an ion (X) to Ca^{2+} concentration in rainwater sample and earth crust, respectively. $[X/Na^+]_{sea}$ and $[X/Ca^{2+}]_{crust}$ ratios were obtained from Keene *et al.* (1986) and Taylor (1964).

The sea-salt fraction (SSF), crustal fraction (CF), and anthropogenic fraction (AF) of each ion measured in rainwater samples could be estimated by using Eqs. (5), (6), and (7), respectively (Keene *et al.*, 1986; Cao *et al.*, 2009; Lu *et al.*, 2011):

$$SSF\ (\%) = 100\frac{[ss - X]}{[X]} = 100\frac{\left[\frac{X}{Na^+}\right]_{sea}\left[Na^+\right]_{rain}}{[X]} \quad (5)$$

$$CF\ (\%) = 100\frac{[c - X]}{[X]} = 100\frac{\left[\frac{X}{Ca^{2+}}\right]_{crust}\left[Ca^{2+}\right]_{rain}}{[X]} \quad (6)$$

$$AF\ (\%) = 100 - SSF - CF \quad (7)$$

where [ss – X] and [c – X] are the sea-salt origin and crustal origin concentrations of an ion in rainwater, respectively; [X] is the concentration of an ion in rainwater; and $[Na^+]_{rain}$ and $[Ca^{2+}]_{rain}$ are the Na^+ and Ca^{2+} concentrations in rainwater, respectively.

The strong acids such as H_2SO_4 and HNO_3 mainly produced from anthropogenic emissions dominate the acidity in wet deposition. Considering that nss-SO_4^{2-} and NO_3^- are two principal acidic components in rainwater, neutralization of acidity can be assessed by fractional acidity (FA). The acidity contributed by H_2SO_4 and HNO_3 is not neutralized at all if FA is equal to unity (Balasubramanian *et al.*, 2001). FA can be estimated using Eq. (8):

$$FA = [H^+]/(([NO_3^-] + [nss\text{-}SO_4^{2-}])) \quad (8)$$

where $[H^+]$ is the H^+ concentration calculated from pH and nss-SO_4^{2-} is the non-sea-salt SO_4^{2-} concentration in rainwater sample.

The free acidity of rainwater resulting from NO_3^- and nss-SO_4^{2-} is buffered by NH_4^+, Ca^{2+}, K^+, and Mg^{2+}. Neutralization factors (NFs) are used to quantitatively reveal the roles of these cations on the neutralization of free acidity in rainwater by using Eqs. (9) and (10) (Possanzini *et al.*, 1988; Kulshrestha *et al.*, 1996):

$$NF_{(X^+)} = \frac{\left[X^+\right]}{\left[NO_3^-\right] + 2\left[nss - SO_4^{2-}\right]} \quad (9)$$

$$NF_{(X^{2+})} = \frac{\left[X^{2+}\right]}{2\left[NO_3^-\right] + \left[nss - SO_4^{2-}\right]} \quad (10)$$

The ratio of neutralizing potential (NP) to acidifying potential (AP) is used to assess the balance between acidity and alkalinity, and it is calculated by Eq. (11) (Alagha and Tuncel, 2003):

$$NP/AP = ([nss\text{-}Ca^{2+}] + [NH_4^+])/([nss\text{-}SO_4^{2-}] + [NO_3^-]) \quad (11)$$

Factor analysis (FA) is a multivariate statistical method that has been frequently used to identify the sources of chemical composition in a wet deposition (Başak and Alagha, 2004; Uygur *et al.*, 2010; Anil *et al.*, 2017). This technique simply separates the variables into groups called *factors* according to their variation and common variance. The obtained factors represent a specific source or mixed sources of the analyzed chemical species. Varimax rotation, the most widely used rotation method, was preferred in rotating the initial factor loadings orthogonally in order to simplify the factor structure and make the factor loadings easily interpretable.

Cluster Analysis of Backward Air Mass Trajectories

The Hybrid Single Particle Lagrangian Integrated Trajectory (HYSPLIT) model (Version 4, 2018 release) was used to compute backward air mass trajectories reaching the receptor site (Calvo *et al.*, 2012; Stein *et al.*, 2015; Rolph *et al.*, 2017).

GDAS (Global Data Assimilation System) 1° HYSPLIT-compatible meteorological data produced by the National Weather Service's National Centers for Environmental Prediction (NCEP) were added to "trajectory setup" (Shi *et al.*, 2014; Xin *et al.*, 2016). The endpoint files of 3-day backward trajectories arriving at 500 m above ground level (AGL) were calculated for every 6 h per day within the study period. 84 backward trajectories were calculated and then classified regarding their typical patterns by using "trajectory clustering analysis" feature of HYSPLIT 4. The software initially calculates 30 clusters, among which the optimum number of clusters is determined by using an objective percent change in total spatial variance (TSV) criterion of either 20% or 30%.

Satellite Observation Data

The satellite observation data of the following parameters over the study period between November 2015 and April 2016 were downloaded from the EARTHDATA GIOVANNI database (Acker and Leptoukh, 2007): i) aerosol optical depth at 0.55 microns for land and ocean (daily 1° [MODIS-Terra MOD08_D3 v6.1]), ii) sea-salt surface mass concentration (monthly 0.5 × 0.625° [MERRA-2 Model M2TMNXAER v5.12.4]), iii) SO_2 surface mass concentration (monthly 0.5 × 0.625° [MERRA-2 Model M2TMNXAER v5.12.4]), and iv) NO_2 tropospheric column (30% cloud screened, daily 0.25° [OMI OMNO2d v003]).

RESULTS AND DISCUSSIONS

Variations of Rainfall, pH, and EC

Time series and correlation statistics of rainfall, duration of rainfall, pH, and EC are demonstrated in Fig. 2 in order to give a preliminary comprehension of the general features of the collected rainwater data. The minimum collected volume of rainfall was 0.36 mm (on Dec. 15) and the maximum was 19.0 mm (on Nov. 25). During the rainy season, the sampling area received less than 25% of the long-term average annual precipitation total of 100 mm. A positive strong correlation between rainfall and duration of rainfall was observed, indicating that rainfall intensity per each rain event was almost steady and has an average of 1.1 ± 1.0 mm h^{-1}. The pH values fluctuating between 6.4 and 8.3 revealed the alkaline nature of rainwater over the study area as the pH of the natural rainwater in equilibrium with atmospheric CO_2 is 5.6 (Granat, 1972). The time series trend of pH is not quite similar to that of rainfall. The correlation between pH and rainfall depth were negative and moderate, which signifies that the pH was partially influenced by rainfall. The EC values varied between 22.7 and 264 µS cm^{-1}, with an average of 126 ± 66.6 µS cm^{-1}. A positive and moderate correlation among pH and EC could be linked to the possible neutralization of acidic constituents by inputs of alkaline substances into rainwater, which will be thoroughly discussed in subsequent sections. The EC of precipitation mainly reflects the total soluble components of the atmosphere which are comparatively bigger in size and tend to be scavenged from the atmosphere more quickly than smaller particles. A major part of the suspended components in the atmosphere is washed out in the first few mm of the precipitation (Anil *et al.*, 2017). For these reasons, the EC value is generally high in the initial stages of the rainfall and gradually drops as the rainfall continues, explaining the negative strong correlation observed among EC and rainfall during the study period.

The monthly variations of rainfall, duration, pH, and EC are depicted in Fig. 3. Even though total durations of rainfall on Nov. 2015 and Dec. 2015 were very close, the total rainfall of Nov. 2015 was twofold higher than that of Dec.

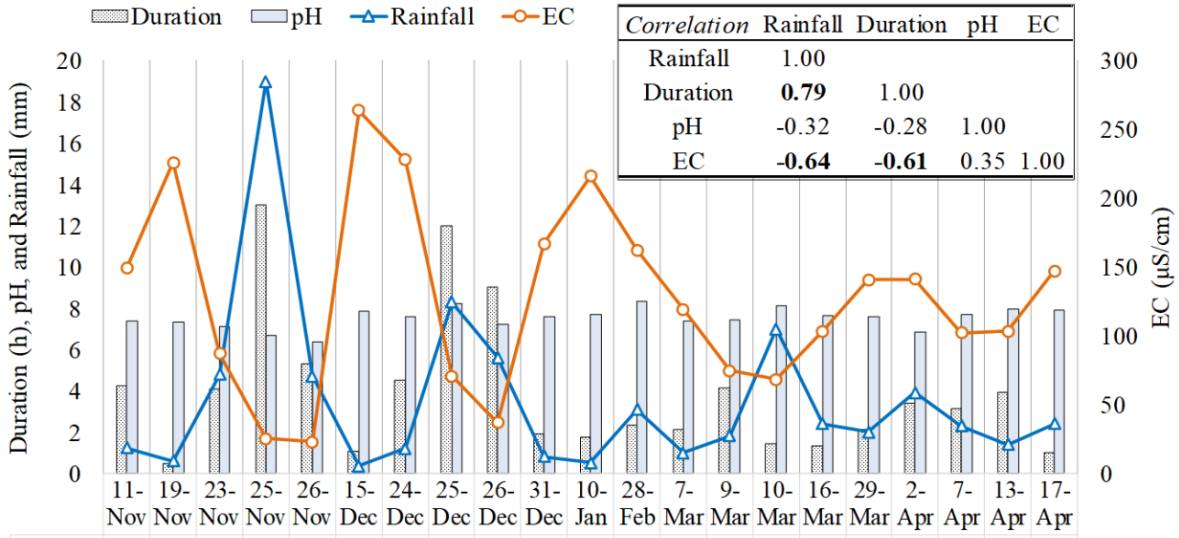

Correlation	Rainfall	Duration	pH	EC
Rainfall	1.00			
Duration	**0.79**	1.00		
pH	-0.32	-0.28	1.00	
EC	**-0.64**	**-0.61**	0.35	1.00

	11-Nov	19-Nov	23-Nov	25-Nov	26-Nov	15-Dec	24-Dec	25-Dec	26-Dec	31-Dec	10-Jan	28-Feb	7-Mar	9-Mar	10-Mar	16-Mar	29-Mar	2-Apr	7-Apr	13-Apr	17-Apr
Duration	4.2	0.5	4.1	13	5.3	1.1	4.5	12	9.0	1.9	1.8	2.3	2.1	4.1	1.4	1.3	2.1	3.4	3.1	3.9	1.0
pH	7.4	7.3	7.1	6.7	6.4	7.8	7.6	8.2	7.2	7.6	7.7	8.3	7.4	7.4	8.1	7.7	7.6	6.8	7.7	8.0	7.9
Rainfall	1.2	0.6	4.8	19	4.7	0.4	1.2	8.3	5.6	0.8	0.5	3.1	1.0	1.8	7.0	2.4	2.0	3.9	2.3	1.4	2.4
EC	149	226	87	25	23	264	228	71	37	167	216	162	119	74	68	103	141	141	102	103	147

Fig. 2. Time series of rainfall, duration, pH, and EC.

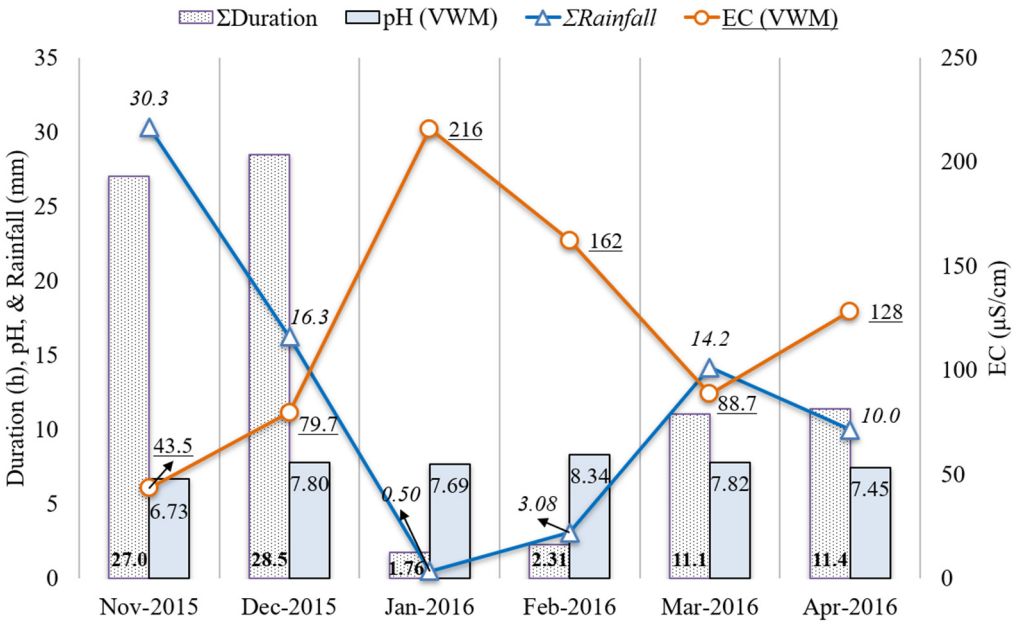

Fig. 3. Monthly variations of rainfall, duration, pH, and EC.

2015 due to the presence of more intense rain events on Nov. 2015. The highest rainfall was recorded on Nov. 2015 with a total depth of 30.3 mm followed by Dec. 2015 (16.3 mm) and Mar 2016 (14.2 mm). Rainfall within these three months accounted for 82% of the total precipitation depth during the study period. In this period, EC values were lower than those of rain events collected on other months (Jan., Feb., and April) due to the dilution effect of abundant rainfall on the total soluble components in the atmospheric column. The negative correlation between rainfall and EC parameters shown in Fig. 3 becomes clearer and stronger (r = –0.94) than that in Fig. 2. On the other hand, the highest EC values were measured as 216 µS cm^{-1} and 162 µS cm^{-1} on Jan. 2016 and Feb. 2016 where the lowest precipitation depths were received. The monthly VWM values of pH showed slight variation during the study period (SD = 0.49) and ranged between 6.73 and 8.34 with an overall VWM of 7.34. The lowest monthly VWM of pH was recorded on Nov. 2015 and accompanied with the highest monthly rainfall total and the lowest EC.

Chemical Composition

The descriptive statistics of the measured parameters in Dammam rainwater such as VWM, mean, median, standard deviation (std. dev.), minimum (min.), maximum (max.), percentiles, and percent distribution of ions in rainwater are listed in Table 2. From the descriptive statistics data, arithmetic means and medians are commonly higher than VWMs, implying that the higher concentrations of ions are usually coupled with lower rainfall amounts. The reason behind this inverse relation could probably be attributed to the dominant wash-out mechanism during the precipitation (Wu *et al.*, 2016; Szép *et al.*, 2018). The high standard deviations of all ions revealed a wide fluctuation of the concentrations in individual precipitation events. The coefficients of variation (Std.Dev/C_{VWM}) of HCO_3^-, Na^+, and NO_3^- were more than the unity, indicating that these ions had larger variations during the study period.

The VWM concentrations of the ions were in the order of $Ca^{2+} > SO_4^{2-} > Cl^- > HCO_3^- > Na^+ > NO_3^- > Mg^{2+} > NH_4^+ > K^+ >> H^+$, revealing that 80% of the rainwater chemical composition was dominated by Ca^{2+}, SO_4^{2-}, Cl^-, HCO_3^-, and Na^+. Following this, the contributions of NO_3^-, Mg^{2+}, NH_4^+, and K^+ to the total ionic composition were 6.93%, 5.95%, 5.88%, and 0.942%, respectively. H^+ was the least abundant ion in the precipitation with the contribution of 0.007%. Among the precipitation components, Ca^{2+} was the most abundant single ion with VWM concentration of 480 µeq L^{-1}, accounted for 30.1% of the total ions and 58.6% of the total cations. The VWM concentration of Ca^{2+} together with Na^+ reached 615 µeq L^{-1}, which explained 75% of the total cation budget in precipitation. The VWM concentration of acidic components, SO_4^{2-} plus NO_3^-, was 466 µeq L^{-1}, occupying 60% of all anions. Marine-originated ions (Na^+ + Cl^-) with VWM concentration of 306 µeq L^{-1} represented 19.2% of the total measured components.

The VWM concentrations of the parameters measured in this study were compared to the literature data from nearby and remote sites in Table 3. Compared to the previous study conducted during 1987 and 1988 (Ahmed *et al.*, 1990), the NH_4^+, SO_4^{2-}, K^+, and Cl^- concentrations increased by 106%, 53%, 31%, and 19%, respectively, whereas NO_3^- indicated 23% reduction. The relative changes in other ions were found to be less than 7%. This is the most interesting to note that the pH value increased from 5.48 to 7.34 in response to decreasing NP/AP ratio from 1.35 to 1.23. In addition to this, the most recent data report demonstrated that SO_2 and NO_x emissions over Saudi Arabia increased 75.6% and 47.7%, respectively, through the years 1988 and 2016 (Crippa *et al.*, 2018). In this regard, one could expect lower pH value and higher NO_3^- concentrations in this current study compared to the previous one. These temporal changes in the precipitation chemistry of study area could be attributed to the variations in:

Table 2. Descriptive statistics of the measured parameters in Dammam's rainwater.

Parameters	Unit	VWM	Mean	Median	Std. Dev.	Min.	Max.	Percentiles			Distribution (%)
								25th	50th	75th	
Rainfall	mm		3.54	2.30	4.17	0.360	19.0	1.10	2.30	4.75	
EC	µS cm^{-1}	77.5	126	119	68.2	22.7	264	72.6	119	165	
pH	pH unit	7.34	7.52	7.61	0.50	6.36	8.34	7.25	7.61	7.87	
Ca^{2+}	µeq L^{-1}	480	817	763	446	55.5	1,679	514	763	1,129	30.1
SO_4^{2-}	µeq L^{-1}	355	476	429	262	66.5	990	284	429	674	22.3
Cl^-	µeq L^{-1}	171	236	195	173	68.0	662	115	195	278	10.7
HCO_3^-	µeq L^{-1}	141	251	262	154	21.1	525	101	262	384	8.81
Na^+	µeq L^{-1}	135	190	167	150	20.2	565	91.0	167	238	8.47
NO_3^-	µeq L^{-1}	111	146	118	77.1	29.0	316	94.3	118	196	6.93
Mg^{2+}	µeq L^{-1}	95.0	127	125	47.3	41.8	206	93.4	125	168	5.95
NH_4^+	µeq L^{-1}	93.8	97.9	92.1	55.1	34.2	200	45.7	92.1	126	5.88
K^+	µeq L^{-1}	15.0	23.3	20.4	12.5	4.86	51.3	13.4	20.4	31.4	0.942
H^+	µeq L^{-1}	0.109	0.062	0.025	0.100	0.005	0.437	0.014	0.025	0.057	0.007

i) atmospheric and meteorological conditions, ii) atmospheric residence times of the ions, iii) mechanisms governing wet scavenging of ions, and iv) long-range transport of air pollutants.

The pH value found in this study was the second highest among those listed in Table 3. The former studies conducted at Saudi Arabia (Riyadh), Jordan, Iran, and Turkey reveal that the pH structure of the Middle East region is alkaline, which is commonly linked to the calcareous soil type of the region, rather than lack of acid-forming ions in the rain (Alabdula'aly and Khan, 2000; Al-Khashman, 2009; Anil *et al.*, 2017; Bayramoğlu Karşı *et al.*, 2018; Naimabadi *et al.*, 2018). The Ca-rich suspended particulate matter over the region, originating from local soil resuspension and long-range particulate matter transport from the Fertile Crescent region and Saharan desert, is the main reason enabling Ca^{2+} to be the most abundant acid-neutralizing component in the regional wet deposition (Ahmed *et al.*, 1990; Alabdula'aly and Khan, 2000). The VWM concentrations of Mg^{2+}, NH_4^+, and K^+, acid-neutralizing species rather than Ca^{2+}, were ranked as the median among those listed in Table 3.

The total concentration of the SO_4^{2-} and NO_3^- in the study area (466 µeq L^{-1}) succeeded the concentrations reported in Ahvaz, Iran (858 µeq L^{-1}); Riyadh, Saudi Arabia (722 µeq L^{-1}); and Bolu, Turkey (487 µeq L^{-1}) (Alabdula'aly and Khan, 2000; Bayramoğlu Karşı *et al.*, 2018; Naimabadi *et al.*, 2018). The higher concentration of total acidic components (SO_4^{2-} + NO_3^-) experienced in Dammam rainwater than those reported for megacities in Turkey (Istanbul), Pakistan (Karachi), India (New Delhi), and China (Beijing) could be attributed to: i) intense burning of fossil fuel for energy production and transportation activities; ii) accumulated SO_4^{2-} and NO_3^- particles on the atmosphere due to limited precipitation and frequent dusty weather conditions, and iii) transboundary pollution.

HCO_3^- was found to be the second most abundant anion in rainwater monitored in Iran, India, Pakistan, Saudi Arabia, Jordan, and Romania (Ahmed *et al.*, 1990; Al-Khashman, 2009; Kumar *et al.*, 2014; Masood *et al.*, 2018; Naimabadi *et al.*, 2018; Szép *et al.*, 2018). HCO_3^- concentration measured in this study (141 µeq L^{-1}) was lower than those observed in Ahvaz, Iran (667 µeq L^{-1}); New Delhi, India (205 µeq L^{-1}); and Karachi, Pakistan (164 µeq L^{-1}).

The equivalent ratio of Na^+/Cl^- must be within the range between 0.5 and 1.5 to indicate a marine origin (Martins *et al.*, 2019). The Na^+/Cl^- ratio found in this study was 0.79 and only 8.1% lower than the seawater ratio of 0.86. The Na^+/Cl^- ratios reported from the sampling sites listed in Table 3 are between 0.5 and 1.5 since they are located close to the coast. The sea-salt aerosol scavenging enriched the Na^+ and Cl^- concentrations in rainwater in those stations except Karachi, Pakistan, and Beijing, China.

The ratio of total cations to total anions ($\sum_{cations}/\sum_{anions}$) of this study was calculated as 1.05, inferring a balance between total cations and total anions. This ratio close to unity gives an indication on neutralization of the rainwater acidity since the most abundant ions of the collected rainwaters samples were Ca^{2+} and SO_4^{2-}. Table 3 reveals that $\sum_{cations}/\sum_{anions}$ ratio of this study was lower than those of many studies except those reported for Turkey, Istanbul (0.81), and Ahvaz, Iran (0.79).

Wet Deposition Fluxes

The monthly variations of the wet deposition fluxes (F_{WD}) of measured ions are presented in Fig. 4. The F_{WD} of acid-neutralizing and soil-derived species (Ca^{2+}, HCO_3^-, NH_4^+, and Mg^{2+}), acidic components (SO_4^{2-} and NO_3^-), and marine-originated ions (Na^+, Cl^-, and K^+) indicated similar temporal trends between each other. The highest F_{WD} of SO_4^{2-}, NO_3^-, Cl^-, Na^+, Mg^{2+}, and K^+ on Nov. 2015 could be linked to the frequent rain events and highest rainfall amount on this period. The F_{WD} of Ca^{2+} and HCO_3^- reached their maximums on Mar 2016 probably due to the higher accumulation of crustal particles appeared during January and February, months in which less rainfall was observed. Besides this, the lowest F_{WD} of all measured ions were recorded on January and February, respectively.

The monthly F_{WD} were strongly correlated ($0.704 < r < 0.986$, $p < 0.01$) with the rainfall amount. In addition to that, a significant linear relationship between the total F_{WD} of each event and the associated rainfall amount was found to be $r = 0.848$ (Fig. 5). It can be concluded from Fig. 5 that rainfall amount significantly contributes to the F_{WD} of ions

Table 3. The VWM concentrations of major parameters in rainwater at selected sites (units are in μeq L^{-1} except pH).

pH	Na^+	K^+	Ca^{2+}	Mg^{2+}	NH_4^+	HCO_3^-	Cl^-	NO_3^-	SO_4^{2-}	Sampling Period	Location	Station Type	Reference
7.34	135	15.0	480	95.0	93.8	141	171	111	355	2015–2016	Dammam, Saudi Arabia	Urban	Current Study
5.48	130	11.5	463	89.5	45.6	151	144	144	233	1987–1988	Dhahran, Saudi Arabia	Urban	Ahmed *et al.* (1990)
7.56	222	42.1	2,192	170	-	-	346	51.0	671	1994	Riyadh, Saudi Arabia	Urban	Alabdula'aly and Khan (2000)
6.91	131	85.2	165	93.1	75.4	134	142	67.3	112	2006–2007	Ghore El-Safi, Jordan	Rural/Industrial	Al-Khashman (2009)
6.00	353	-	806	64.4	320	667	420	127	731	2014–2015	Ahvaz, Iran	Urban	Naimabadi *et al.* (2018)
6.84	484	132	333	97.2	123	164	242	27.1	397	2008	Karachi, Pakistan	Urban	Masood *et al.* (2018)
6.45	54.5	33.5	328	32.5	252	205	92.5	112	214	2010–2011	New Delhi, India	Urban	Kumar *et al.* (2014)
5.99	160	48.3	1,287	141	53.8	-	146	153	334	2014	Bolu, Turkey	Urban	Bayramoğlu Karşı *et al.* (2018)
6.05	93.0	12.4	109	31.4	20.1	-	143	59.0	125	2009	Istanbul, Turkey	Urban	Anil *et al.* (2017)
6.40	26.4	27.7	203	19.2	201	54.2	45.2	39.1	159	2006–2016	Carpathians, Romania	Rural/Industrial	Szép *et al.* (2018)
7.00	127	151	489	124	504	-	153	243	220	2009–2013	Po Valley, Italy	Semi-Rural	Tositti *et al.* (2017)
4.85	21.5	9.17	273	53.3	346	-	50.9	42.6	357	2011–2012	Beijing, China	Urban	Xu *et al.* (2015)

since the total ionic F_{WD} exhibited a similar fluctuation tendency with the rainfall amount as shown in Fig. 5. In the meantime, the F_{WD} of major chemical components over the study area was also affected by the temporal variations of emissions from crustal, marine, and anthropogenic sources.

The total F_{WD} of the ions during the study period were in the order of SO_4^{2-} (1,269 mg m^{-2}) > Ca^{2+} (714 mg m^{-2}) > HCO_3^- (638 mg m^{-2}) > NO_3^- (510 mg m^{-2}) > Cl^- (450 mg m^{-2}) > Na^+ (231 mg m^{-2}) > NH_4^+ (126 mg m^{-2}) > Mg^{2+} (85.8 mg m^{-2}) > K^+ (43.7 mg m^{-2}) > H^+ (8 μg m^{-2}). During the study period, the Dammam metropolitan area received a total ionic F_{WD} of 4.07 tons per km^2 which was lower than those reported in Po Valley, Italy (43.3 tons km^{-2} y^{-1}) (Tositti *et al.*, 2017); Beijing, China (23.3 tons km^{-2} y^{-1}) (Xu *et al.*, 2015); Karachi, Pakistan (16.8 tons km^{-2} y^{-1}) (Masood *et al.*, 2018) Istanbul, Turkey (9.01 tons km^{-2} y^{-1}) (Anil *et al.*, 2017); Carpathians, Romania (7.13 tons km^{-2} y^{-1}) (Szép *et al.*, 2018); and Ahvaz, Iran (4.57 tons km^{-2} y^{-1}) (Naimabadi *et al.*, 2018). Consequently, rare precipitation events with low-volume rainfalls experienced in arid and semiarid regions such as Saudi Arabia commonly cause higher concentrations of ions in rainwater and lower annual F_{WD} of ions relative to the wetter regions receiving more frequent rain events with larger volumes (Keene *et al.*, 2015).

Acid Neutralization

The pH value of the rainwater is mainly controlled by the neutralization between acidic and basic components. The fractional acidity (FA), correlations between acidic and alkaline species, SO_4^{2-}/NO_3^- ratio, and neutralization factors (NFs) are the most well-known approaches to clarify the factors governing the acid neutralization in rainwater. The mean FA value of all rainwater samples was calculated to be 0.0003 ± 0.001, revealing that 99.97% of the acidity had been neutralized by alkaline species. The positive and strong linear correlation between ($[Ca^{2+}] + [Mg^{2+}] + [NH_4^+] + [K^+]$) and ($[SO_4^{2-}] + [NO_3^-]$) (r = 0.894) also supports that the alkaline species measured in the study were responsible for the neutralization of the rainwater acidity and the contribution of any other alkaline components to the neutralization process was not significant. The relative contributions of SO_4^{2-} and NO_3^- in the precipitation acidity can be evaluated by using the equivalent ratio of $[SO_4^{2-}]/([NO_3^-] + [SO_4^{2-}])$. The mean value of this ratio during the study period was 0.756 ± 0.039, reflecting that about 75.6% of rainwater acidity was due to SO_4^{2-} while the contribution of NO_3^- was 24.4%. Comparing to the former study, the equivalent $[SO_4^{2-}]/[NO_3^-]$ ratio has increased from 1.61 to 3.21 since 1990, indicating that H_2SO_4 has an increasing effect on the precipitation acidity in Dammam (Ahmed *et al.*, 1990). The NFs of Ca^{2+}, Mg^{2+}, NH_4^+, and K^+ were calculated in order to evaluate the rainwater neutralization by alkaline components in detail. The Ca^{2+} showed the highest NF value (1.09) and followed by Mg^{2+} (0.135), NH_4^+ (0.117), and K^+ (0.02). These results suggest that Ca^{2+} was the principal neutralizer in rainwater and its contribution to the total neutralization was about 80%. Furthermore, Ca^{2+} plays a dominant role in the neutralization process of rainwater in the Middle East due to the Ca-rich soil structure of the region.

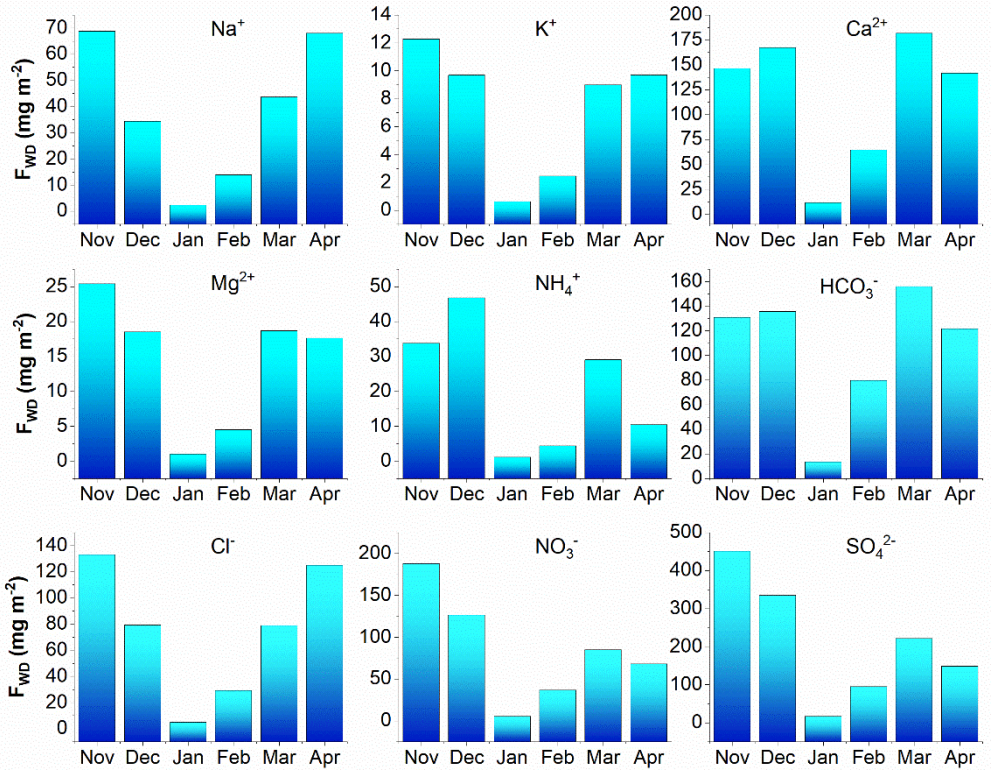

Fig. 4. Monthly variations of wet deposition fluxes.

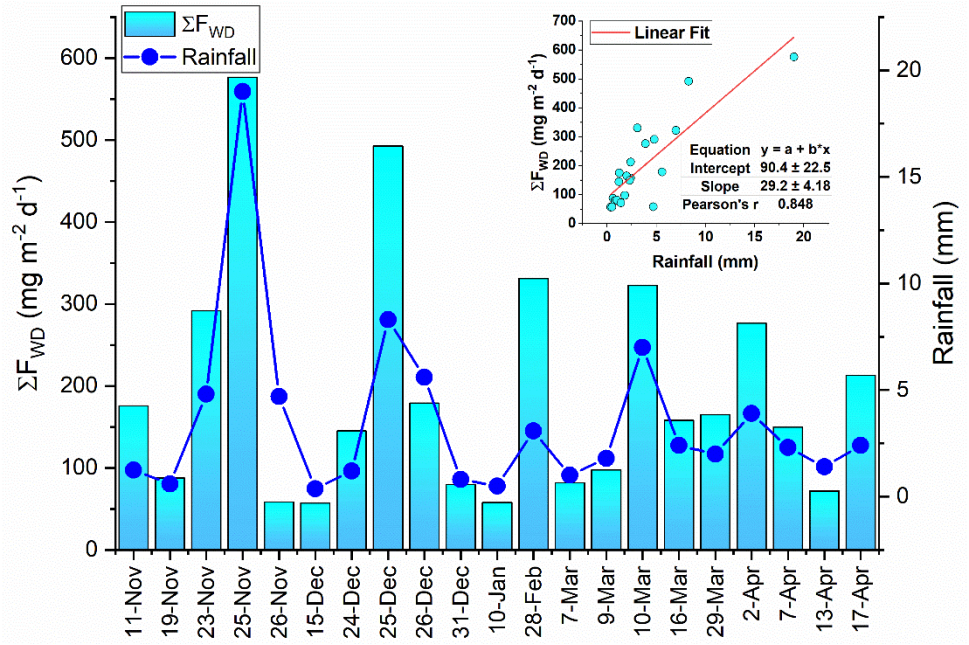

Fig. 5. Time series of total ionic wet deposition fluxes.

Source Apportionment

Enrichment Factors and Relative Source Contributions

The enrichment factor (EF) model, a double normalization technique, has been used to determine possible sources of ions in rainwater (Başak and Alagha, 2004). An EF value of an ion much less than 1 or much higher than 1 is assumed to be diluted or enriched in regard to the reference source (Al-Momani *et al.*, 1997). In this study, Na^+ was selected as a marine reference ion since average equivalent ratios of $[Cl^-]/[Na^+]$ and $[Mg^{2+}]/[Na^+]$ in rainwater samples were higher than those in standard seawater (Zhang *et al.*, 2012). Ca and Al are commonly used as a soil reference element to identify the crustal origin of elements in rainwater (Okay *et al.*, 2002). Ca^{2+} was selected

as a crustal reference since Al was not measured in the rainwater samples. The mean values of marine enrichment factors (EF_m) and crustal enrichment factors (EF_c) of ions are given in Table 4. The EF_m of NO_3^- was not calculated since its abundance in standard seawater is very meager (Cao *et al.*, 2009).

The EF_m and EF_c values of Cl^- were found to be 1.20 and 389, respectively, indicating that the origin of Cl^- in rainwater was mainly sea-salt particles due to the proximity of the sampling location to the western coast of Arabian Gulf. The EF_m of Cl^- was slightly higher than the recommended seawater ratio of 1.16, which could be proof of possible terrestrial contribution. The EF_m and EF_c values of K^+ and Mg^{2+} reveal that these ions were slightly enriched compared to seawater and diluted to earth crust. These results indicated that K^+ and Mg^{2+} mostly originated from crustal sources and partly from marine sources. The high EF_m of Ca^{2+} (117) showed that marine contribution to Ca^{2+} was negligible and crustal-originated particles were the main source of Ca^{2+} in rainwater. The contributions of NO_3^- and SO_4^{2-} to rainwater were not mainly from marine or crustal sources since the EF_c value of NO_3^- and the EF_m and EF_c values of SO_4^{2-} were all much higher than 10.

The approximate sea-salt fraction (SSF), crustal fraction (CF), and anthropogenic fraction (AF) of each ionic component in rainwater were estimated by using Eqs. (5), (6), and (7) and shown in Table 5. In this study, Na^+ was assumed to be of purely marine origin. Table 5 shows that 90.1% of Cl^- originated from sea-salt particles, 9.19% from anthropogenic sources, and only 0.705% from earth crust. Ca^{2+}, K^+, and Mg^{2+} in rainwater were mainly of crustal origin whereas their CFs were calculated to be 98.7%, 82.0%, and 68.7%, respectively. The contribution from marine sources to Mg^{2+} accounting for 31.3% was also considerable in comparison with other region-specific tracer cations of the earth crust. The terrestrial contribution to these three cations could be ascribed to only earth crust because it is very difficult to differentiate their crustal and anthropogenic sources with the available rainwater data (Cao *et al.*, 2009; Xiao, 2016). The anthropogenic sources indicated the highest effect on NO_3^- and SO_4^{2-} in rainwater with a contribution of 99.6% and 93.0%, respectively. The SSF and CF of SO_4^{2-} were estimated to be 5.67% and 1.37%, respectively. Apart from AF, NO_3^- in rainwater had a very slight contribution only from crustal sources. In Saudi Arabia, road transportation, public electricity and heat production, manufacturing industries, and construction sectors were reported to be the most significant emission sources of atmospheric NO_x and SO_2 which are precursors of anthropogenic NO_3^- and SO_4^{2-} in regional rainwater (Ahmed *et al.*, 1990; Alabdula'aly and Khan, 2000; Crippa *et al.*, 2018).

Factor Analysis

In this study, "principal components method" and "eigenvalues greater than 1" options were selected during the extraction of factors using SPSS ver. 24. Three major factors with eigenvalues higher than unity were extracted and the results are given in Table 6. The extracted factors explained 92.6% of the total variance of the dataset. The communalities of all variables were higher than 0.855, indicating that the extracted factors are reasonable.

Factor 1 explaining 51% of the total variance is the most significant factor and characterized by high loadings of Ca^{2+}, K^+, Mg^{2+}, HCO_3^-, SO_4^{2-}, and NO_3^-. This group of ions describes mixed sources since it includes crustal markers and anthropogenic components. The surface soil structure of the study area and the region typically contains limestone ($CaCO_3$ and $CaMg(CO_3)_2$) and is partially interbedded with feldspar (Al_2SiO_5 of K or CaO), gypsum ($CaSO_4 \cdot 2H_2O$), and halite (NaCl) (Alsaaran, 2008). Considering this information, it can be inferred that accumulated coarse particles on the atmosphere due to resuspension of local soil by surface wind and long-range particulate transport from nearby deserts on North Africa, Fertile Crescent region, and Arabian Peninsula are the main sources of the enriched crustal cations, particularly Ca^{2+} in Dammam's rainwater. The calcium bicarbonate ($Ca(HCO_3)_2$) is formed as a result of the reaction between the dissolved CO_2 in rainwater and $CaCO_3$. This soluble compound is eventually washed out from the atmosphere

Table 5. Marine and terrestrial contributions to ions in Dammam's rainwater.

Ions	Source fractions (%)		
	Marine	Terrestrial	
		Crustal	Anthropogenic
Na^+	100		
K^+	18.0	82.0	
Ca^{2+}	1.29	98.7	
Mg^{2+}	31.3	68.7	
Cl^-	90.1	0.705	9.19
NO_3^-		0.385	99.6
SO_4^{2-}	5.67	1.37	93.0

Table 4. Enrichment factors of ions in Dammam's rainwater relative to standard seawater and earth crust.

	K^+	Mg^{2+}	Ca^{2+}	Cl^-	SO_4^{2-}
Rainwater (X/Na^+)	0.154	0.898	5.12	1.39	3.20
Seawater (X/Na^+)	0.022	0.227	0.044	1.16	0.121
EF_m	7.05	3.96	117	1.20	26.5
	K^+	Mg^{2+}	$^*NO_3^-$	Cl^-	$^*SO_4^{2-}$
Rainwater (X/Ca^{2+})	0.068	0.136	0.830	0.702	1.99
Earth crust (X/Ca^{2+})	0.504	0.561	0.002	0.003	0.019
EF_c	0.135	0.241	389	224	106

*Crustal N and S regarded as the entire NO_3^- and SO_4^{2-} compounds, respectively (from Taylor, 1964).

Table 6. Factor analysis results of ions in the precipitation of Dammam.

Variable	Factor 1	Factor 2	Factor 3	Communality
Na^+		0.960		0.988
K^+	0.801	0.432		0.855
Ca^{2+}	0.955			0.972
Mg^{2+}	0.784	0.483		0.878
NH_4^+			0.957	0.950
HCO_3^-	0.937			0.894
Cl^-		0.952		0.985
NO_3^-	0.793		0.400	0.889
SO_4^{2-}	0.877		0.451	0.921
Eigenvalue	5.81	1.64	1.08	
Variance (%)	51.0	28.0	13.6	
Possible source	Mixed	Marine	Anthropogenic	

Only moderate and significant factor loadings ≥ 0.4 and ≤ 0.4 are shown.

by wet deposition (Kulshrestha *et al.*, 2003; Demirak *et al.*, 2006). The considerable abundance of HCO_3^- in Dammam's rainwater, 8.81% of total chemical composition, and a strong correlation between Ca^{2+} and HCO_3^- (r = 0.889) unveil two different scenarios that complement each other: i) $CaCO_3$-rich particles over the atmosphere during the rain events and ii) the presence of elevated CO_2 emissions to the atmosphere due to the burning of fossil fuels during the study period. The coexistence of SO_4^{2-} and NO_3^- in this factor and strong correlation between these acidic components (r = 0.951) could be linked to their similar chemical behaviors in the atmosphere and common sources of their precursors SO_2 and NO_x. It was reported that emissions of SO_2 and NO_x in Saudi Arabia in 2016 were 3.37 Mt and 1.84 Mt, respectively (Crippa *et al.*, 2018). Public electricity, heat production, and other energy industries were responsible for 78% of SO_2 emissions while the contributions of the energy sector and road transportation to NO_x emissions were 62% and 27%, respectively. The significant correlations between the acidifying components and crustal cations in this factor could be attributed to neutralizing reactions between H_2SO_4 and HNO_3, and alkaline compounds in rainwater. Therefore, SO_4^{2-} and NO_3^- in the precipitation mostly existed as the forms of $CaSO_4$ and $Ca(NO_3)_2$ in this study whereas Ca^{2+} was responsible for 80% of the total neutralization in collected rainwater samples (see Section: "Acid Neutralization").

The second factor accounting for 28.0% of the total variance indicated high loadings of Na^+ and Cl^- and moderate loadings of Mg^{2+} and K^+. This factor clearly describes the marine source and the incorporation of sea-salt particles into rainwater. In this study, the source of the Na^+ in rainwater was assumed to be totally from the sea and the correlation coefficients of this ion with Cl^-, Mg^{2+}, and K^+ were found to be 0.995, 0.661, and 0.575, respectively. The estimated SSF fractions of Cl^- (90.1%), Mg^{2+} (31.3%), and K^+ (18.0) from the previous section also supports the dominance of Na^+-Cl^- couple and partial effects of Mg^{2+} and K^+ in this factor. Mg^{2+} and K^+ have higher loadings in Factor 1, explaining that their origins in rainwater were mainly from crustal sources and partly from marine sources. The existence of Cl^- with a weak loading (0.267) in Factor 1 could explain its anthropogenic fraction (9.19%) possibly due to emissions from fossil fuel combustion, burning of waste materials, and automobile exhaust within the study area (Palmer, 1976; Wu *et al.*, 2016; Szép *et al.*, 2018).

Factor 3 represents 13.6% of the total variance with high loading of NH_4^+ and moderate loadings of SO_4^{2-} and NO_3^-. Atmospheric NH_4^+ mainly originates from anthropogenic sources such as agricultural activities, fertilizer factories, biomass burning, and emissions from vehicles. The atmospheric NH_3 reacts rapidly with H_2SO_4 and HNO_3 to form secondary fine particles of $(NH_4)_2SO_4$ and NH_4NO_3. In this neutralization reaction, the reaction of NH_3 with H_2SO_4 is favored over reaction with HNO_3. Since the atmospheric settling velocity of SO_4^{2-} particles is slower than NH_3 and HNO_3, fine $(NH_4)_2SO_4$ particles dominate the distribution of atmospheric NH_4^+ over longer distances (NOAA, 2000). In this regard, the higher factor loading of SO_4^{2-} compared to NO_3^- in this factor suggests that $(NH_4)_2SO_4$ particles could be more abundant than NH_4NO_3 particles over the study area. The possible sources of NH_4^+ in Dammam's rainwater might be resulting from: i) local NH_3 emissions from vehicles but not from other local sources since agricultural activities and biomass burning are quite limited in the study area and ii) long-range transport of secondary fine particles of $(NH_4)_2SO_4$ and NH_4NO_3 over the regions where SO_2, NO_x, and NH_3 emissions are intense.

Cluster Analysis Coupled with Satellite Observations

The cluster analysis of backward air mass trajectories arriving at the sampling area for the rainy days of the study period resulted in a 7-cluster solution. This was determined as the optimum number of clusters regarding its TSV changes among other cluster solutions. The percentages of the classified 3-day backward air mass trajectories, clustered rain event codes, and total F_{WD} values of ions in each cluster were calculated and shown in Table 7. The obtained satellite observation data of aerosol optical depth at 0.55 microns, sea-salt surface mass concentration, SO_2 surface mass concentration, NO_2 tropospheric column (30% cloud screened), and the average backward air mass trajectories in 7-cluster solution were visualized for the same domain (Region 9E, 15N, 60E, 45N) by using ArcGIS ver. 10.3 and depicted in Fig. 6.

Table 7. Cluster statistics and total F_{WD} of ions (kg km^{-2}) in each cluster.

Cluster	Trajectory Frequency (%)	Clustered rain event code	Na^+	K^+	Ca^{2+}	Mg^{2+}	NH_4^+	HCO_3^-	Cl^-	NO_3^-	SO_4^{2-}	$\sum F_{WD}$
Cluster 1	17.9	2, 4, 7, 8	55.2	11.2	151	25.5	50.1	117	111	217	563	1,302
Cluster 2	9.52	6, 13	5.51	1.73	30.8	2.45	3.91	24.4	10.5	17.0	42.5	139
Cluster 3	15.5	10, 12, 19, 20	24.4	7.09	133	10.7	13.5	147	49.2	74.3	172	632
Cluster 4	8.33	11, 16	11.6	1.73	48.7	4.67	4.11	52.2	21.4	21.5	49.7	216
Cluster 5	22.6	3, 9, 14, 15, 21	63.8	13.5	237	25.9	43.8	204	121	108	286	1,103
Cluster 6	13.1	1, 18	57.4	6.16	75.2	10.3	5.11	44.9	104	50.9	98.7	452
Cluster 7	13.1	5, 17	13.3	2.33	37.2	6.39	5.01	47.8	33.3	21.7	56.2	223

During the study period, 53% of the observed precipitation events were mainly controlled by the air masses in Clusters 2, 4, 5, and 6 arriving at the sampling site from north-northwest (NNW) sector. Even though Clusters 2, 4, and 6 arose from different regions, they followed a similar pathway with Cluster 5 for about 24 h before their arrival to the sampling area. Their common trajectory started from southern Iraq, traversed Kuwait and Arabian Gulf, respectively, and they reached Dammam from NNW direction. According to their longer pathways among others, Clusters 4 and 6 originating from central Tunisia and Black Sea region of Turkey, respectively, were ascribed to fast-moving trajectories with the mean altitudes of 2,412 m and 2,019 m, respectively. On the other hand, trajectories with a mean altitude of 1,333 m in Cluster 5 were the slowest ones among northwesterly clusters. The air masses deriving from the west-southwest (WSW) sector and arriving at Dammam from northeast (NE) direction were attributed to Cluster 1. This group of trajectories with a mean altitude of 1,650 m representing 18% of all rain systems of the study could be characterized as marine- and terrestrial-impacted nationwide cluster as they originated from the Red Sea coast of Jeddah, passed over Western Province, Riyadh, and Arabian Gulf coast of the study region. The rain systems in Clusters 3 and 7 reaching the sampling site from southerly directions accounted for 29% of all precipitation events. The trajectories in Cluster 7 deriving from Oman transported over southeast (SE) part of Saudi Arabia, the western section of United Arab Emirates, Arabian Gulf, Qatar, Bahrain, and eventually reached over Dammam from southeast (SE) direction. The rain systems in this cluster could be enriched by marine and terrestrial sources throughout their trajectories. Cluster 3 representing 16% of the total back trajectories originated from 50 km off the Dammam shoreline (on the Arabian Gulf side), made a circular motion in a clockwise direction around Qatar, entered the land border of Saudi Arabia between Qatar and United Arab Emirates, and completed its circular motion by reaching the sampling point from south direction. Among all clusters, this distinctive group of trajectories was identified as the slowest- and lowest-altitude-moving ones due to their shortest range and lowest mean altitude (673 m AGL).

Clusters 1, 3, and 5 describing 56% of the total back trajectories dominated 75% of the total F_{WD} during the study period. The rain systems in Cluster 1 represented 32% of the total F_{WD}, including the highest depositions of anthropogenic ions (SO_4^{2-}, NO_3^-, and NH_4^+) and high depositions of crustal and sea-salt components on the study area (Table 7). The potential long-range and medium-range sources of the highest depositions of these anthropogenic ions were highly populated and heavily industrialized cities throughout the route of Cluster 1 such as Western Province and Riyadh where high emissions of SO_2 and NO_2 were observed (Figs. 6(c) and 6(d)). The southern part of Saudi Arabia indicated moderate to high aerosol optical depth values within the map domain after hot spots over Chad, Niger, and Oman (Fig. 6(a)), which could be attributed to the high F_{WD} of crustal ions brought by air masses in this cluster. The back trajectories deriving over the Red Sea have potentials to transport high quantities of Na^+ and Cl^- to the study area due to the highest sea-salt concentrations observed over the Red Sea throughout the map domain (Fig. 6(b)).

Cluster 5 representing the highest fraction of the total back trajectories (23% of total) accounted for 27% of the total F_{WD} over the study area. The rain events associated with the air masses from this cluster were characterized by the highest F_{WD} of both crustal and sea-salt components and also high F_{WD} of anthropogenic ions due to high particle loads and high emissions of SO_2 and NO_2 over southern Iraq, Kuwait, and the Dammam metropolitan area and also moderate sea-salt mass concentration over the Arabian Gulf throughout the pathway of their travel. In addition to this, the slow- and medium-altitude-moving characteristic of the air masses in this cluster resulted in efficient transport and better enrichment of the species in the atmospheric columns along the route from southern Iraq to the receptor point. Among the source regions, Kuwait was possibly the most important contributor to the F_{WD} of anthropogenic components since it was the highest SO_2 and NO_2 emitter within this cluster.

Similar to Cluster 5, atmospheric species within the path of Cluster 3 were efficiently acquired by the rain clouds and deposited over the receptor area as this cluster grouped the slowest- and lowest-altitude-moving air masses and indicated more local characteristics as well. This cluster explaining 16% of the back trajectories represented the third highest F_{WD} of both crustal and anthropogenic ions and medium sea-salt enrichment as well. Apart from the local effects on the total F_{WD}, eastern part of Qatar emitting considerable amounts of NO_2 partially contributed to F_{WD} of NO_3^-.

Even though Clusters 2, 4, 6, and 7 together described 44% of the total back trajectories, the regions that were passed over by all these clusters contributed only 25% to the

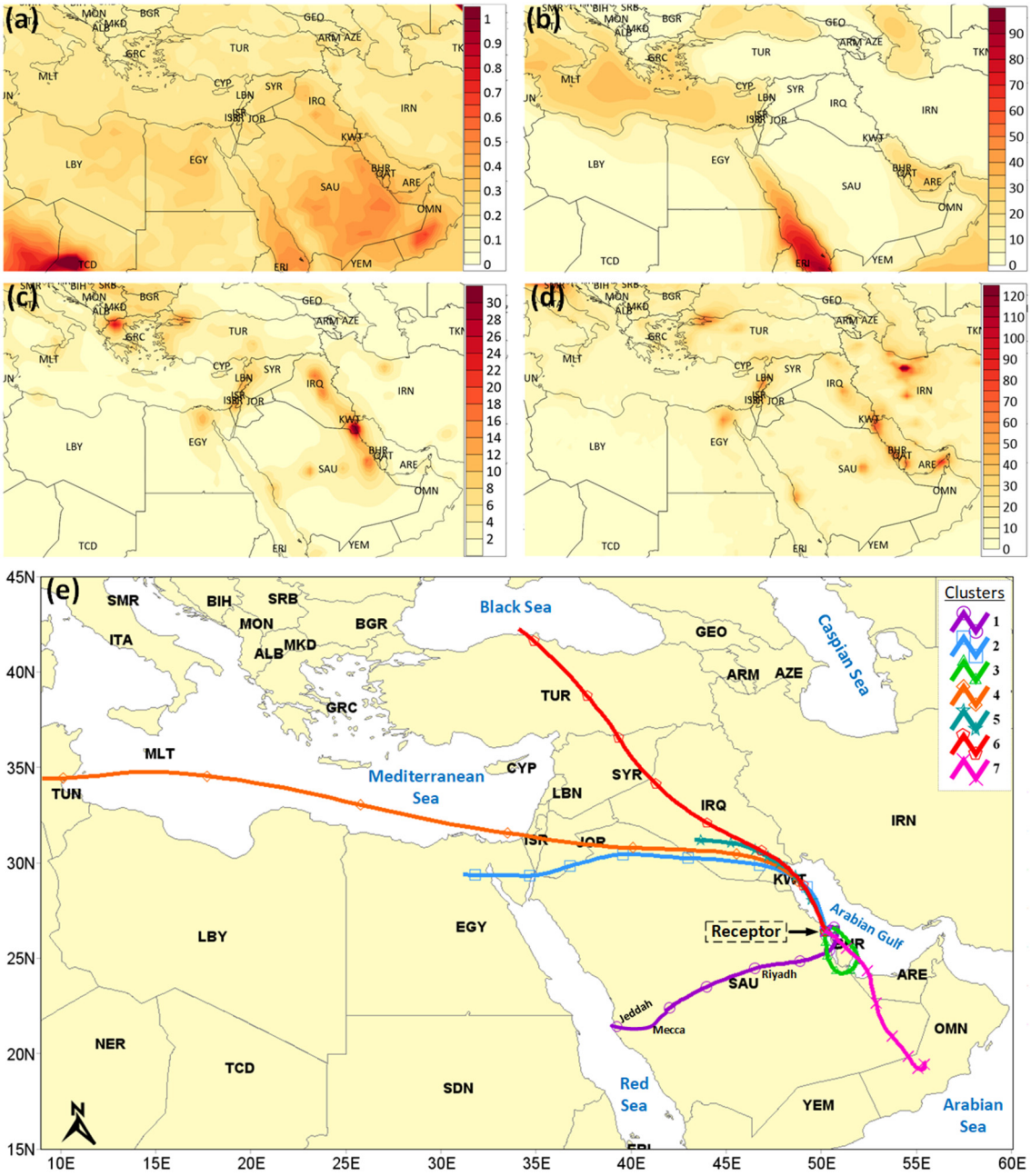

Fig. 6. (a) Aerosol optical depth at 0.55 micron for land and ocean, (b) sea-salt surface mass concentration (μg m^{-3}), (c) SO_2 surface mass concentration (μg m^{-3}), (d) NO_2 tropospheric column (1×10^{-14} cm^{-2}), and (e) average 3-day backward trajectories arriving at 500 m AGL in 7-cluster solution.

total F_{WD} over the study area. This could be attributed to: i) limited enrichment capacities of fast- and high-altitude moving systems in Clusters 2, 4, and 6 by atmospheric species on the atmospheric columns that they were passing through and ii) low trajectory frequencies of the individual clusters. Among these four clusters, air masses in Cluster 6 showed the highest contribution (11%) to the total F_{WD}. About quarter of both Na^+ and Cl^-, 14% of K^+, 12% of Mg^{2+}, 11% of Ca^{2+}, 10% of NO_3^-, and 8% of SO_4^{2-} in total F_{WD} corresponded to the rain systems in Cluster 6. The source locations of the sea-salt ions enriched together were substantially from the Arabian Gulf and partially from the central Black Sea region of Turkey where the air masses in this cluster originated. Like in Cluster 5, the anthropogenic emissions from Iraq and especially from Kuwait were the long-range origins of NO_3^- and SO_4^{2-} deposited to the sampling area by rain systems in Cluster 6. The crustal components transported by Cluster 6 could be attributed to the medium particle loads over Iraq and Kuwait shown in Fig. 6(a).

CONCLUSIONS

21 samples of rainwater, which totaled 74 mm in rainfall

depth, were collected by an automatic wet-only precipitation sampler during the rainy season between November 2015 and April 2016 in Dammam, Saudi Arabia. The VWM value of the pH was found to be 7.34 (± 0.49), indicating the alkaline nature of the rainwater in the study area. The chemical composition of the rainwater was dominated by Ca^{2+}, SO_4^{2-}, Cl^-, HCO_3^-, and Na^+, which accounted for 80% of the total ionic equivalent concentration. Ca^{2+}, with a VWM concentration of 480 μeq L^{-1}, was the most abundant ion and contributed 30.1% of the total ionic equivalent concentration. During the study period, the Dammam metropolitan area received a total ionic F_{WD} of 4.07 tons per km^2, which consisted of the following components in descending order: $SO_4^{2-} > Ca^{2+} > HCO_3^- > NO_3^- > Cl^- > Na^+ > NH_4^+ > Mg^{2+} > K^+$.

The concentration of the combined SO_4^{2-} and NO_3^- in the study area (466 μeq L^{-1}) was higher than those reported for megacities in Turkey, Pakistan, India, and China. Approximately 75.6% of the rainwater acidity was due to SO_4^{2-} and 24.4%, to NO_3^-. The extremely low fractional acidity of the rainwater indicated that almost all of the acidity was neutralized by alkaline species, with Ca^{2+} being responsible for 80% of the samples' neutralization, revealing that SO_4^{2-} and NO_3^- were mostly present as $CaSO_4$ and $Ca(NO_3)_2$ in the precipitation.

Source apportionment based on enrichment factor, relative source contribution, and factor analysis as well as cluster analysis coupled with satellite observations showed that the anthropogenic components (SO_4^{2-}, NO_3^-, and NH_4^+), which contributed 47% of the total ionic F_{WD}, mainly arose from i) the intensive burning of fossil fuel for energy production and transportation activities in the vicinity of the study area and ii) the medium-range and long-range transport of anthropogenic pollutants from Kuwait, Iraq, Qatar, the Western Province, and Riyadh. Local soil resuspension, moderate to high particulate matter loads over the southern part of Saudi Arabia, and long-range transport from Iraq and Kuwait contributed the crustal components (Ca^{2+}, HCO_3^-, K^+, and Mg^{2+}), which accounted for 36% of the total ionic F_{WD}. Finally, the marine components, Na^+ and Cl^-, which primarily originated in the Arabian Gulf, with smaller contributions from the coast of the Red Sea in Jeddah and the central Black Sea region of Turkey, formed 17% of the total ionic FWD.

In this study, we developed a new method that combined satellite observations and cluster analysis of backward air mass trajectories to determine the potential source regions for the chemical components in Dammam's rainwater. This technique was proven to be an effective tool for investigating the source receptor relationships of atmospheric air pollutants.

ACKNOWLEDGMENT

This study was supported by the Deanship of Scientific Research at Imam Abdulrahman Bin Faisal University with the grant numbers 2011-067-Eng and 2012-165-Eng. The authors gratefully acknowledge the NOAA Air Resources Laboratory (ARL) for the provision of the HYSPLIT transport and dispersion model and/or READY website (http://www.ready.noaa.gov) used in this publication. The authors deeply acknowledge the Goddard Earth Sciences Data and Information Services Center (GES DISC) for the satellite data downloaded from EARTHDATA GIOVANNI website (https://giovanni.gsfc.nasa.gov).

CONFLICT OF INTEREST

The authors declare no conflict of interest.

REFERENCES

Acker, J.G. and Leptoukh, G. (2007). Online analysis enhances use of NASA Earth science data. *Eos, Trans AGU* 88: 14–17.

Ahmed, A.F.M., Singh, R.P. and Elmubarak, A.H. (1990). Chemistry of atmospheric precipitation at the Western Arabian Gulf Coast. *Atmos. Environ.* 24: 2927–2934.

Akkoyunlu, B.O., Oruc, I. and Tayanc, M. (2011). The chemistry of wet deposition flux in Istanbul, Turkey. In *International multidisciplinary scientific geoscience*, Libadmin, L. (Ed.), The World Source of Geosciences, Bulgaria, pp. 1255–1262.

Alabdula'aly, A.I. and Khan, M.A. (2000). Chemistry of rain water in Riyadh, Saudi Arabia. *Arch. Environ. Contam. Toxicol.* 39: 66–73.

Alagha, O. and Tuncel, G. (2003). Evaluation of air quality over the black sea major ionic composition of rainwater. *Water Air Soil Pollut. Focus* 3: 89–98.

Al-Daghri, N.M., Alokail, M.S., Abd-Alrahman, S.H., Draz, H.M., Yakout, S.M. and Clerici, M. (2013). Polycyclic aromatic hydrocarbon exposure and pediatric asthma in children: A case-control study. *Environ. Health* 12: 1–6.

Al-Daghri, N.M., Alokail, M.S., Abd-Alrahman, S.H. and Draz, H.M. (2014). Polycyclic aromatic hydrocarbon distribution in serum of Saudi children using HPLC-FLD: marker elevations in children with asthma. *Environ. Sci. Pollut. Res. Int.* 21: 12085–12090.

Al-Khashman, O.A. (2009). Chemical characteristics of rainwater collected at a western site of Jordan. *Atmos. Res.* 91: 53–61.

Al-Momani, I.F., Ataman, O.Y., Anwari, M.A., Tuncel, S., Köse, C. and Tuncel, G. (1995a). Chemical composition of precipitation near an industrial area at Izmir, Turkey. *Atmos. Environ.* 29: 1131–1143.

Al-Momani, I.F., Tuncel, S., Eler, Ü., Örtel, E., Sirin, G. and Tuncel, G. (1995b). Major ion composition of wet and dry deposition in the eastern Mediterranean basin. *Sci. Total Environ.* 164: 75–85.

Al-Momani, I.F., Güllü, G., Ölmez, I., Eler, Ü., Örtel, E., Sirin, G. and Tuncel, G. (1997). Chemical composition of eastern Mediterranean aerosol and precipitation: Indications of long-range transport. *Pure Appl. Chem.* 69: 41–46.

Al-Momani, I.F., Momani, K.A. and Jaradat, Q.M. (2000). Chemical composition of wet precipitation in Irbid, Jordan. *J. Atmos. Chem.* 35: 47–57.

Al-Refeai, T. and Al-Ghamdy, D. (1994). Geological and geotechnical aspects of Saudi Arabia. *Geotech. Geol. Eng.* 12: 253–276.

Alsaaran, N.A. (2008). Origin and geochemical reaction paths of sabkha brines: Sabkha Jayb Uwayyid, eastern Saudi Arabia. *Arabian J. Geosci.* 1: 63–74.

Al-Saleh, I., Alsabbahen, A., Shinwari, N., Billedo, G., Mashhour, A., Al-Sarraj, Y., Mohamed Gel, D. and Rabbah, A. (2013). Polycyclic aromatic hydrocarbons (PAHs) as determinants of various anthropometric measures of birth outcome. *Sci. Total Environ.* 444: 565–578.

Anil, I., Alagha, O. and Karaca, F. (2017). Effects of transport patterns on chemical composition of sequential rain samples: Trajectory clustering and principal component analysis approach. *Air Qual. Atmos. Health* 10: 1193–1206.

Balasubramanian, R., Victor, T. and Chun, N. (2001). Chemical and statistical analysis of precipitation in Singapore. *Water Air Soil Pollut.* 130: 451–456.

Başak, B. and Alagha, O. (2004). The chemical composition of rainwater over Büyükçekmece Lake, Istanbul. *Atmos. Res.* 71: 275–288.

Bayramoğlu Karşı, M.B., Yenisoy-Karakaş, S. and Karakaş, D. (2018). Investigation of washout and rainout processes in sequential rain samples. *Atmos. Environ.* 190: 53–64.

Bouwman, A.F., Van Vuuren, D.P., Derwent, R.G. and Posch, M. (2002). A global analysis of acidification and eutrophication of terrestrial ecosystems. *Water Air Soil Pollut.* 141: 349–382.

Budhavant, K.B., Rao, P.S.P., Safai, P.D. and Ali, K. (2009). Chemistry of monsoon and post-monsoon rains at a high altitude location, Sinhagad, India. *Aerosol Air Qual. Res.* 9: 65–79.

Burns, D.A., Aherne, J., Gay, D.A. and Lehmann, C.M.B. (2016). Acid rain and its environmental effects: Recent scientific advances. *Atmos. Environ.* 146: 1–4.

Calvo, A.I., Pont, V., Olmo, F.J., Castro, A., Alados-Arboledas, L., Vicente, A.M., Fernández-Raga, M. and Fraile, R. (2012). Air masses and weather types: A Useful tool for characterizing precipitation chemistry and wet deposition. *Aerosol Air Qual. Res.* 12: 856–878.

Cao, Y.Z., Wang, S., Zhang, G., Luo, J. and Lu, S. (2009). Chemical characteristics of wet precipitation at an urban Site of Guangzhou, South China. *Atmos. Res.* 94: 462–469.

Crippa, M., Guizzardi, D., Muntean, M., Schaaf, E., Dentener, F., van Aardenne, J.A., Monni, S., Doering, U., Olivier, J.G.J., Pagliari, V. and Janssens-Maenhout, G. (2018). Gridded emissions of air pollutants for the period 1970–2012 within EDGAR V4.3.2. *Earth Syst. Sci. Data* 10: 1987–2013.

Demirak, A., Balci, A., Karaoglu, H. and Tosmur, B. (2006). Chemical characteristics of rain water at an urban site of south western Turkey. *Environ. Monit. Assess.* 123: 271–283.

DeNicola, E., Aburizaiza, O.S., Siddique, A., Khwaja, H. and Carpenter, D.O. (2015). Climate change and water scarcity: The case of Saudi Arabia. *Ann. Global Health* 81: 342–353.

de Moraes Dias, V.R., Sanches, L., de Carvalho Alves, M. and de Souza Nogueira, J. (2012). Spatio-temporal variability of anions in wet precipitation of Cuiabá, Brazil. *Atmos. Res.* 107: 9–19.

Driscoll, C.T., Lawrence, G.B., Bulger, A.J., Butler, T.J., Cronan, C.S., Eagar, C., Lambert, K.F., Likens, G.E., Stoddard, J.L. and Weathers, K.C. (2001). Acidic deposition in the northeastern U.S.: Sources and inputs, ecosystems effects, and management strategies. *BioScience* 51: 180–198.

El-Mubarak, A.H., Rushdi, A.I., Al-Mutlaq, K.F., Bazeyad, A.Y., Simonich, S.L.M. and Simoneit, B.R.T. (2014). Occurrence of high levels of persistent organic pollutants (POPs) in particulate matter of the ambient air of Riyadh, Saudi Arabia. *Arabian J. Sci. Eng.* 40: 81–92.

EMEP (2013). Report: Transboundary Acidification, Eutrophication and Ground Level Ozone in Europe in 2011. Technical Report No: EMEP Report 1/2013. The European Monitoring and Evaluation Programme, Norway.

Facchini Cerqueira, M.R., Pinto, M.F., Derossi, I.N., Esteves, W.T., Rachid Santos, M.D., Costa Matos, M.A., Lowinsohn, D. and Matos, R.C. (2014). Chemical characteristics of rainwater at a southeastern site of Brazil. *Atmos. Pollut. Res.* 5: 253–261.

Gaga, E.O. and Ari, A. (2011). Gas–particle partitioning of polycyclic aromatic hydrocarbons (PAHs) in an urban traffic site in Eskisehir, Turkey. *Atmos. Res.* 99: 207–216.

GAW (2004). Report: Manual for the Global Atmosphere Watch Precipitation Chemistry Programme. Technical Report No: 160. World Meteorology Organization - Global Atmosphere Watch. Geneva, Switzerland.

Granat, L. (1972). On the relation between pH and the chemical composition in atmospheric precipitation. *Tellus* 24: 550–560.

Kant, S., Panda, J. and Manoj, M.G. (2019). A satellite observation-based analysis of aerosol-cloud-precipitation interaction during the february 2016 unseasonal heatwave episode over Indian region. *Aerosol Air Qual. Res.* 19: 1508–1525.

Keene, W.C., Galloway, J.N., Likens, G.E., Deviney, F.A., Mikkelsen, K.N., Moody, J.L. and Maben, J.R. (2015). Atmospheric wet deposition in remote regions: Benchmarks for environmental change. *J. Atmo.s Sci.* 72: 2947–2978.

Keene, W.C., Pszenny, A.A.P., Galloway, J.N. and Hawley, M.E. (1986). Sea-salt corrections and interpretation of constituent ratios in marine precipitation. *J. Geophys. Res.* 91: 6647–6658.

Kulshrestha, U.C., Sarkar, A.K., Srivastava, S.S. and Parashar, D.C. (1996). Investigation into atmospheric deposition through precipitation studies at New Delhi (India). *Atmos. Environ.* 30: 4149–4154.

Kulshrestha, U.C., Kulshrestha, M.J., Sekar, R., Sastry, G.S.R. and Vairamani, M. (2003). Chemical characteristics of rainwater at an urban site of south-central India. *Atmos. Environ.* 37: 3019–3026.

Kumar, P., Yadav, S. and Kumar, A. (2014). Sources and processes governing rainwater chemistry in New Delhi, India. *Nat. Hazards* 74: 2147–2162.

Li, Y.C., Zhang, M., Shu, M., Ho, S.S., Liu, Z.F., Wang, X.X. and Zhao, X.Q. (2016). Chemical characteristics of

rainwater in Sichuan basin, a case study of Ya'an. *Environ. Sci. Pollut. Res. Int.* 23: 13088–13099.

Likens, G.E. (1987). Chemical wastes in our atmosphere—An ecological crisis. *Ind. Crisis Q.* 1: 13–33.

Lu, X., Li, L.Y., Li, N., Yang, G., Luo, D. and Chen, J. (2011). Chemical characteristics of spring rainwater of Xi'an city, NW China. *Atmos. Environ.* 45: 5058–5063.

Martins, E.H., Nogarotto, D.C., Mortatti, J. and Pozza, S.A. (2019). Chemical composition of rainwater in an urban area of the southeast of Brazil. *Atmos. Pollut. Res.* 10: 520–530.

Mashat, A. and Abdel Basset, H. (2011). Analysis of rainfall over Saudi Arabia. *J. King Abdulaziz Univ. Met. Environ. Arid Land Agric. Sci.* 22: 59–78.

Masood, S.S., Saied, S., Siddique, A., Mohiuddin, S., Hussain, M.M., Khan, M.K. and Khwaja, H.A. (2018). Influence of urban–coastal activities on organic acids and major ion chemistry of wet precipitation at a metropolis in Pakistan. *Arabian J. Geosci.* 11: 1–15.

Michelsen, N., Reshid, M., Siebert, C., Schulz, S., Knöller, K., Weise, S.M., Rausch, R., Al-Saud, M. and Schüth, C. (2015). Isotopic and chemical composition of precipitation in Riyadh, Saudi Arabia. *Chem Geol* 413: 51–62.

Naimabadi, A., Shirmardi, M., Maleki, H., Teymouri, P., Goudarzi, G., Shahsavani, A., Sorooshian, A., Babaei, A.A., Mehrabi, N., Baneshi, M.M., Zarei, M.R., Lababpour, A. and Ghozikali, M.G. (2018). On the chemical nature of precipitation in a populated Middle Eastern Region (Ahvaz, Iran) with diverse sources. *Ecotoxicol. Environ. Saf.* 163: 558–566.

Nasser, L.A. (2005). Occurrence of terrestrial fungi in accumulated rainfall water in Saudi Arabia *J. King Saud Univ.* 18: 63–72.

NOAA (2000). Report: Atmospheric Ammonia: Sources and Fate. NOAA - National Oceanic and Atmospheric Administration. Broadway, Boulder Colorado, USA.

Notaro, M., Alkolibi, F., Fadda, E. and Bakhrjy, F. (2013). Trajectory analysis of Saudi Arabian dust storms. *J. Geophys. Res.* 118: 6028–6043.

Okay, C., Akkoyunlu, B.O. and Tayanc, M. (2002). Composition of wet deposition in Kaynarca, Turkey. *Environ. Pollut.* 118: 401–410.

Palmer, T.Y. (1976). Combustion sources of atmospheric chlorine. *Nature* 263: 44–46.

Possanzini, M., Buttini, P. and Di Palo, V. (1988). Characterization of a rural area in terms of dry and wet deposition. *Sci. Total Environ.* 74: 111–120.

Rolph, G., Stein, A. and Stunder, B. (2017). Real-time environmental applications and display system: READY. *Environ. Modell. Software* 95: 210–228.

Romero Orué, M., Gaiero, D. and Kirschbaum, A. (2019). Seasonal characteristics of the chemical composition of rainwaters from Salta city, NW Argentina. *Environ. Earth Sci.* 78: 1–9.

Schemenauer, R.S. and Cereceda, P. (1992). Monsoon cloudwater chemistry on the Arabian Peninsula. *Atmos. Environ.* 26: 1583–1587.

Shi, P., Xie, P.H., Qin, M., Si, F.Q., Dou, K. and Du, K. (2014). Cluster analysis for daily patterns of SO_2 and NO_2 measured by the DOAS system in Xiamen. *Aerosol Air Qual. Res.* 14: 1455–1465.

Stein, A.F., Draxler, R.R., Rolph, G.D., Stunder, B.J.B., Cohen, M.D. and Ngan, F. (2015). NOAA's HYSPLIT atmospheric transport and dispersion modeling system. *Bull. Am. Meteorol. Soc.* 96: 2059–2077.

Szep, R., Mateescu, E., Nechifor, A.C. and Keresztesi, A. (2017). Chemical characteristics and source analysis on ionic composition of rainwater collected in the Carpathians "Cold Pole," Ciuc basin, Eastern Carpathians, Romania. *Environ. Sci. Pollut. Res. Int.* 24: 27288–27302.

Szép, R., Mateescu, E., Niță, I.A., Birsan, M.V., Bodor, Z. and Keresztesi, Á. (2018). Effects of the eastern carpathians on atmospheric circulations and precipitation chemistry from 2006 to 2016 at four monitoring stations (Eastern Carpathians, Romania). *Atmos. Res.* 214: 311–328.

Taylor, S.R. (1964). Abundance of chemical elements in the continental crust: A new table. *Geochim. Cosmochim. Acta* 28: 1273–1285.

Tiwari, S., Hopke, P.K., Thimmaiah, D., Dumka, U.C., Srivastava, A.K., Bisht, D.S., Rao, P.S.P., Chate, D.M., Srivastava, M.K. and Tripathi, S.N. (2016). Nature and sources of ionic species in precipitation across the Indo-Gangetic Plains, India. *Aerosol Air Qual. Res.* 16: 943–957.

Tositti, L., Pieri, L., Brattich, E., Parmeggiani, S. and Ventura, F. (2017). Chemical characteristics of atmospheric bulk deposition in a semi-rural area of the Po Valley (Italy). *J. Atmos. Chem.* 75: 97–121.

Tsai, Y.I., Kuo, S.C., Young, L.H., Hsieh, L.Y. and Chen, P.T. (2014). Atmospheric dry *plus* wet deposition and wet-only deposition of dicarboxylic acids and inorganic compounds in a coastal suburban environment. *Atmos. Environ.* 89: 696–706.

Uygur, N., Karaca, F. and Alagha, O. (2010). Prediction of sources of metal pollution in rainwater in Istanbul, Turkey using factor analysis and long-range transport models. *Atmos. Res.* 95: 55–64.

Vlastos, D., Antonopoulou, M., Lavranou, A., Efthimiou, I., Dailianis, S., Hela, D., Lambropoulou, D., Paschalidou, A.K. and Kassomenos, P. (2019). Assessment of the toxic potential of rainwater precipitation: First evidence from a case study in three Greek cities. *Sci. Total Environ.* 648: 1323–1332.

Wedyan, M.A. (2013). Characterization of dissolved organic nitrogen (DON) in rainwater of Qassim, Saudi Arabia *World J. Appl. Sci. Res.* 3: 1–7.

Whelpdale, D.M., Summers, P.W. and Sanhueza, E. (1997). A global overview of atmospheric acid deposition fluxes. *Environ. Monit. Assess.* 48: 217–247.

Wu, Y., Xu, Z., Liu, W., Zhao, T., Zhang, X., Jiang, H., Yu, C., Zhou, L. and Zhou, X. (2016). Chemical compositions of precipitation at three non-urban sites of Hebei Province, North China: Influence of terrestrial sources on ionic composition. *Atmos. Res.* 181: 115–123.

Wu, Y., Zhang, J., Ni, Z., Liu, S., Jiang, Z. and Huang, X. (2018). Atmospheric deposition of trace elements to Daya Bay, South China Sea: Fluxes and sources. *Mar. Pollut.*

Bull. 127: 672–683.

Xiao, J. (2016). Chemical composition and source identification of rainwater constituents at an urban site in Xi'an. *Environ. Earth Sci.* 75: 209.

Xin, Y., Wang, G. and Chen, L. (2016). Identification of long-range transport pathways and potential sources of PM_{10} in Tibetan Plateau uplift area: Case study of Xining, China in 2014. *Aerosol Air Qual. Res.* 16: 1044–1054.

Xu, Z., Wu, Y., Liu, W.J., Liang, C.S., Ji, J., Zhao, T. and Zhang, X. (2015). Chemical composition of rainwater and the acid neutralizing effect at Beijing and Chizhou City, China. *Atmos. Res.* 164–165: 278–285.

Zhang, N., He, Y., Cao, J., Ho, K. and Shen, Z. (2012). Long-term trends in chemical composition of precipitation at Lijiang, southeast Tibetan Plateau, southwestern China. *Atmos. Res.* 106: 50–60.

Received for review, May 3, 2019
Revised, September 16, 2019
Accepted, October 23, 2019